Ultrafast strong-field absorption in gapped graphene

S. Azar Oliaei Motlagh [ORCID],[*] Ahmal Jawad Zafar [ORCID], Aranyo Mitra [ORCID], Vadym Apalkov, and Mark I. Stockman
Center for Nano-Optics (CeNO) and Department of Physics and Astronomy, Georgia State University, Atlanta, Georgia 30303, USA

We study theoretically the strong-field absorption of an ultrafast optical pulse by a gapped graphene monolayer. At low field amplitudes, the absorbance in pristine graphene is equal to the universal value of 2.3%. Although the ultrafast optical absorption for low field amplitudes is independent of the polarization, linear or circular, of the applied optical pulse, for high field amplitudes, the absorption strongly depends on the pulse polarization. For a linearly polarized pulse, the optical absorbance is saturated at the value of $\approx 1.4\%$ for the pulse's amplitude of $\geqslant 0.4$ V/Å, but no such saturation is observed for a circularly polarized pulse. For the gapped graphene, the absorption of a linearly polarized pulse shows a weak dependence on the bandgap, while for a circularly polarized pulse, the absorption is very sensitive to the bandgap.

I. INTRODUCTION

The progress in generation of ultrafast intense laser pulses provides powerful tools to observe the highly nonlinear, strong-field phenomena in solids and expand the field of strong-field optics to both small time scales and high field intensities [1–15]. Some of these strong-field phenomena are high-harmonic generation, ultrafast ionization, nonlinear current generation, and nonlinear optical absorption [16–21].

Graphene is a well-known two-dimensional solid made of a single layer of carbon atoms [22–27]. It has a honeycomb crystal structure with two inequivalent sublattices, *A* and *B* [22,24]. The first Brillouin zone of graphene is a hexagon and the corresponding energy dispersion is gapless at two Dirac points, *K* and *K*′, with a massless relativistic energy dispersion [22,24,28,29]. The electron states at the Dirac points are chiral. They are characterized by nontrivial Berry phases $\pm\pi$, which are opposite at the *K* and *K*′ points [14,30–32]. The corresponding Berry curvature is nonzero only at the Dirac points, at which it has a δ-type singularity. For other two-dimensional materials with a honeycomb crystal structure but with a finite bandgap, such as monolayers of transition-metal dichalcogenides, the Berry curvature is nonzero within finite regions near the *K* and *K*′ points with the maxima at these points [14,32]. Thus, opening the bandgap in graphenelike materials broadens the Berry curvature in the *K* and *K*′ valleys. This broadening results in the effect of topological resonance [33], which occurs during ultrafast electron dynamics and is due to the compensation of the dynamic phase and the topological phase.

The gapped graphene has a broken inversion symmetry: the point symmetry group decreases from D_{6h} for graphene to D_{3h}. Consequently, a bandgap opens up at the *K* points. Previously, we have shown that, due to the existence of the bandgap, topological resonance appears in strong fields.

Consequently, a femtosecond intense optical pulse generates a large valley polarization [33], which is not related to the electron spin or the spin-orbit coupling.

Also, in the gapped graphene, in addition to the field-driven longitudinal current, there is a transverse current in the direction normal to the applied field [34]. This transverse current is also due to the breaking of the inversion symmetry; consequently, it depends greatly on the bandgap.

One of the important characteristics of the interaction of an optical pulse with solids is the absorption coefficient. For pristine graphene, in the linear regime, approximately 2.3% of the incident light energy is absorbed. In sharp contrast, nonlinear absorption, which was measured for an 80-fs optical pulse, showed saturable behavior [19–21]. For such a long pulse, the electron dynamics in the field of the pulse is incoherent, and scattering and relaxation processes are important. Here, we study absorption by gapped graphene for an ultrashort optical pulse, with a duration of just a few femtoseconds. For such a short pulse, the electron dynamics is coherent, and the system exhibits new features related to the topological resonance. To describe different types of graphenelike materials, we consider the model of gapped graphene with a variable bandgap. The bandgap can be opened, for example, by applying a staggered potential, which can be realized by epitaxially growing graphene on a SiC substrate [35].

II. MODEL AND MAIN EQUATIONS

We consider electron dynamics in the field of a pulse with a duration of just a few femtoseconds. Taking into account that electron scattering times in graphene are of the order of or longer than 10 fs (see Refs. [36–41]), we neglect electron collisions and assume that the electron dynamics is coherent. Such dynamics is described by the time-dependent Schrödinger equation (TDSE),

$$i\hbar\frac{d\Psi_{\alpha\mathbf{q}}}{dt} = H(t)\Psi_{\alpha\mathbf{q}}, \quad H(t) = H_0 - e\mathbf{F}(t)\mathbf{r}, \quad (1)$$

*soliaeimotlagh1@gsu.edu

where $\mathbf{F}(t)$ is the electric field of the pulse, and e is the electron charge. Here we assume that the electron initially (before the pulse) is in the band α [$\alpha =$ v for the valence band (VB) and $\alpha =$ c for the conduction band (CB)] with crystal momentum $\mathbf{q}$.

The field-free Hamiltonian H_0 is the nearest-neighbor two-band tight-binding Hamiltonian of gapped graphene [42–45],

$$H_0 = \begin{pmatrix} \Delta_g/2 & \gamma f(\mathbf{k}) \\ \gamma f^*(\mathbf{k}) & -\Delta_g/2 \end{pmatrix}, \qquad (2)$$

where Δ_g is the bandgap, $\gamma = -3.03$ eV is the hopping integral, and

$$f(\mathbf{k}) = \exp\left(i\frac{ak_y}{\sqrt{3}}\right) + 2\exp\left(-i\frac{ak_y}{2\sqrt{3}}\right)\cos\left(\frac{ak_x}{2}\right), \quad (3)$$

where $a = 2.46$ Å is the lattice constant.

The energies of the CB and VB can be found from Hamiltonian H_0 and are given by the expression

$$E_\alpha(\mathbf{k}) = \pm\sqrt{\gamma^2|f(\mathbf{k})|^2 + \Delta_g^2/4}\,, \qquad (4)$$

where the signs $\pm$ stand for CB ($\alpha = c$) and VB ($\alpha = v$), respectively.

The applied electric field generates both intraband and interband electron dynamics. The intraband dynamics is described by the Bloch acceleration theorem [46], which determines the time-dependent electron wave vector, $\mathbf{k}(\mathbf{q}, t)$, as

$$\mathbf{k}(\mathbf{q}, t) = \mathbf{q} + \frac{e}{\hbar}\int_{-\infty}^{t}\mathbf{F}(t')dt', \qquad (5)$$

where $\mathbf{q}$ is the initial electron wave vector. In relation to the Bloch trajectories, (5), we also define the separatrix as a set of initial points $\mathbf{q}$ for which the electron trajectories pass precisely through the corresponding K or K' points [47]. Its parametric equation is

$$\mathbf{q}(t) = \mathbf{K} - \mathbf{k}(0, t) \quad \text{or} \quad \mathbf{q}(t) = \mathbf{K}' - \mathbf{k}(0, t), \qquad (6)$$

where $t \in (-\infty, \infty)$ is a parameter.

To determine the the intraband electron dynamics, we solve the TDSE in terms of the Houston functions [48], which are adiabatic solutions for intraband dynamics,

$$\Phi_{\alpha\mathbf{q}}^{(\mathrm{H})}(\mathbf{r}, t) = \Psi_{\mathbf{k}(\mathbf{q},\mathbf{t})}^{(\alpha)}(\mathbf{r})\exp\left(i\phi_\alpha^{(\mathrm{d})}(\mathbf{q}, t) + i\phi_\alpha^{(\mathrm{B})}(\mathbf{q}, t)\right), \quad (7)$$

where $\Psi_{\mathbf{k}(\mathbf{q},\mathbf{t})}^{(\alpha)}$ are the Bloch functions. Here the dynamic phase, $\phi_\alpha^{(\mathrm{D})}$, and the geometrical phase, $\phi_\alpha^{(\mathrm{B})}$, are defined as

$$\phi_\alpha^{(\mathrm{D})}(\mathbf{q}, t) = \frac{-1}{\hbar}\int_{-\infty}^{t}dt'(E_\alpha[\mathbf{k}(\mathbf{q}, t')]), \qquad (8)$$

$$\phi_\alpha^{(\mathrm{B})}(\mathbf{q}, t) = \frac{-e}{\hbar}\int_{-\infty}^{t}dt'\mathbf{F}(\mathcal{A}^{\alpha\alpha}[\mathbf{k}(\mathbf{q}, t')]). \qquad (9)$$

In Eq. (9), $\mathcal{A}^{\alpha\alpha} = \langle\Psi_\mathbf{q}^{(\alpha)}|i\frac{\partial}{\partial\mathbf{q}}|\Psi_\mathbf{q}^{(\alpha)}\rangle$ is the intraband Berry connection for band α, which in this model can be found analytically as

$$\mathcal{A}_x^{cc}(\mathbf{k}) = \frac{-a\gamma^2}{\gamma^2|f(\mathbf{k})|^2 + (\Delta_g/2 - E_c)^2}\sin\frac{3ak_y}{2\sqrt{3}}\sin\frac{ak_x}{2}, \qquad (10)$$

$$\mathcal{A}_y^{cc}(\mathbf{k}) = \frac{a\gamma^2}{\sqrt{3}(\gamma^2|f(\mathbf{k})|^2 + (\Delta_g/2 - E_c)^2)}$$
$$\times\left(\cos ak_x - \cos\frac{\sqrt{3}ak_y}{2}\cos\frac{ak_x}{2}\right), \quad (11)$$

$$\mathcal{A}_x^{vv}(\mathbf{k}) = \frac{-a\gamma^2}{\gamma^2|f(\mathbf{k})|^2 + (\Delta_g/2 + E_c)^2}\sin\frac{3ak_y}{2\sqrt{3}}\sin\frac{ak_x}{2}, \qquad (12)$$

$$\mathcal{A}_y^{vv}(\mathbf{k}) = \frac{a\gamma^2}{\sqrt{3}(\gamma^2|f(\mathbf{k})|^2 + (\Delta_g/2 + E_c)^2)}$$
$$\times\left(\cos ak_x - \cos\frac{\sqrt{3}ak_y}{2}\cos\frac{ak_x}{2}\right). \quad (13)$$

The general solution of TDSE (1) can be expanded in the basis of the Houston functions as

$$\Psi_\mathbf{q}(\mathbf{r}, t) = \sum_{\alpha=c,v}\beta_{\alpha\mathbf{q}}(t)\Phi_{\alpha\mathbf{q}}^{(\mathrm{H})}(\mathbf{r}, t), \qquad (14)$$

where $\beta_{\alpha\mathbf{q}}$ are the expansion coefficients, which satisfy the following system of coupled differential equations:

$$i\hbar\frac{\partial B_\mathbf{q}(t)}{\partial t} = H'(\mathbf{q}, t)B_\mathbf{q}(t). \qquad (15)$$

Here the wave function (the vector of state) $B_q(t)$ and Hamiltonian in the interaction representation $H'(\mathbf{q}, t)$ are defined as

$$B_\mathbf{q}(t) = \begin{bmatrix}\beta_{c\mathbf{q}}(t) \\ \beta_{v\mathbf{q}}(t)\end{bmatrix}, \qquad (16)$$

$$H'(\mathbf{q}, t) = -e\mathbf{F}(t)\hat{\mathcal{A}}(\mathbf{q}, t), \qquad (17)$$

$$\hat{\mathcal{A}}(\mathbf{q}, t) = \begin{bmatrix}0 & \mathcal{D}^{cv}(\mathbf{q}, t) \\ \mathcal{D}^{vc}(\mathbf{q}, t) & 0\end{bmatrix}. \qquad (18)$$

The non-Abelian Berry connection matrix elements, $\mathcal{A}^{cv} = (\mathcal{A}_x^{cv}, \mathcal{A}_y^{cv})$, which are proportional to the interband dipole matrix elements, are given by the expressions

$$\mathcal{A}_x^{cv}(\mathbf{k}) = \mathcal{N}\left(\frac{-a}{2|f(\mathbf{k})|^2}\right)\left(\sin\frac{ak_x}{2}\sin\frac{a\sqrt{3}k_y}{2}\right.$$
$$\left. + i\frac{\Delta_g}{2E_c}\left(\cos\frac{a\sqrt{3}k_y}{2}\sin\frac{ak_x}{2} + \sin ak_x\right)\right), \quad (19)$$

$$\mathcal{A}_y^{cv}(\mathbf{k}) = \mathcal{N}\left(\frac{a}{2\sqrt{3}|f(\mathbf{k})|^2}\right)\left(-1 - \cos\frac{a\sqrt{3}k_y}{2}\cos\frac{ak_x}{2}\right.$$
$$\left. + 2\cos^2\frac{ak_x}{2} - i\frac{3\Delta_g}{2E_c}\sin\frac{a\sqrt{3}k_y}{2}\cos\frac{ak_x}{2}\right), \quad (20)$$

where

$$\mathcal{N} = \frac{|\gamma f(\mathbf{k})|}{\sqrt{\frac{\Delta_g^2}{4} + |\gamma f(\mathbf{k})|^2}}. \qquad (21)$$

In the presence of a strong field, we solve TDSE (15) with the initial conditions that the VB is initially fully occupied and the CB is completely empty. From these solutions we can find the residual CB population and find the energy absorbed by the graphene monolayer. The corresponding absorbance is
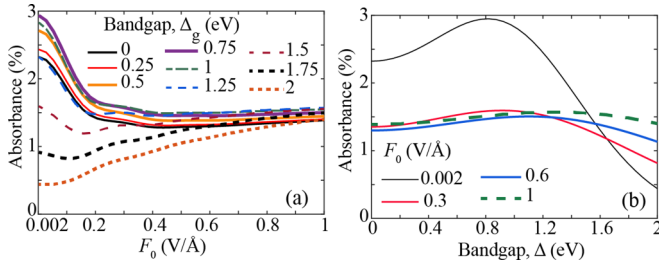
FIG. 1. Absorbance in gapped graphene (a) as a function of the field amplitude for $\Delta_g = 0$, 0.25, 0.5, 0.75, 1, 1.25, 1.5, 1.75, and 2 eV and (b) as a function of the bandgap for $F_0 = 0.002$, 0.3, 0.6, and 1 V/Å. The applied optical pulse is linearly polarized along the x direction.

defined as

$$A = \frac{\int |\beta_{c\mathbf{q}}(t=\infty)|^2 E_c(\mathbf{q}) d\mathbf{q}}{2\pi^2 c \epsilon_0 \int_{-\infty}^{\infty} |\mathbf{F}|^2 dt}, \tag{22}$$

where c is the speed of light in vacuum, and ϵ_0 is the dielectric permittivity of the surrounding medium.

Below we present the results for a gapped graphene monolayer for both linearly and circularly polarized pulses.

III. RESULTS

A. Linearly polarized ultrafast pulse

First, we consider a linearly polarized optical pulse that consists of a single oscillation and is polarized along the x axis (zigzag direction), $\mathbf{F}(t) = (F_x(t), 0)$. The waveform of this pulse is set as

$$F_x(t) = F_0(1 - 2u^2) \exp(-u^2), \tag{23}$$

where F_0 is the amplitude of the pulse, $u = t/\tau$, and $\tau = 1$ fs is the characteristic time of the optical oscillation.

The calculated absorbance as a function of the field amplitude is shown in Fig. 1 for different values of the bandgap, Δ_g. For the pristine graphene, $\Delta_g = 0$, the absorbance takes the universal value of $\pi\alpha \approx 2.3\%$ ($\alpha = \frac{1}{137}$ is the fine-structure constant) for field amplitudes as low as 0.002 V/Å.

With increasing field amplitude, F_0, the absorbance decreases for small Δ_g, $\Delta_g \lesssim 1.5$ eV, and increases for large Δ_g, $\Delta_g \gtrsim 1.5$ eV. Finally, it reaches the saturated value of $\approx 1.5\%$ at $F_0 \gtrsim 0.5$ V/Å [see Fig. 1(a)]. Visible suppression of absorbance at small Δ_g with increasing field amplitude can be understood by looking at the CB population distribution for different field amplitudes, 0.002, 0.2, 0.6, and 1 V/Å; see Fig. 2, which shows the results for pristine graphene.

The CB population distribution is determined by the properties of the interband dipole matrix element (non-Abelian Berry connection). Namely, for pristine graphene, the x component of the interband dipole matrix element has singularities at the Dirac points, K and K', of type $q_y/(q_x^2 + q_y^2)$, where (q_x, q_y) is the wave vector defined relative to the corresponding Dirac point. Thus the interband coupling, in this case, is strongly localized at the Dirac points. As a result, if during the pulse an electron passes through the region that is very close to the Dirac point, then strongly localized interband coupling rotates the electron pseudospin by 180°. This means that if
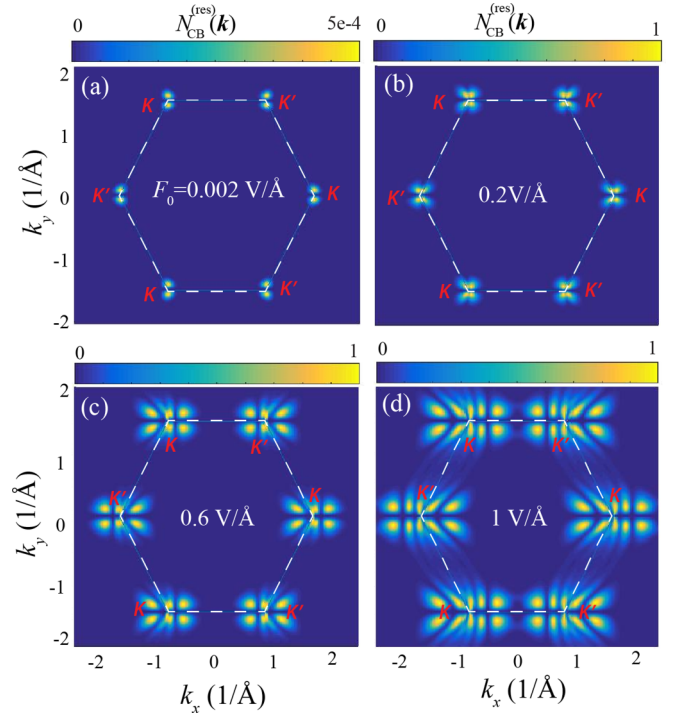

FIG. 2. Residual CB population of graphene with $\Delta_g = 0$ induced by a linearly polarized pulse in the x direction. The field amplitude is (a) 0.002 V/Å, (b) 0.2 V/Å, (c) 0.6 V/Å, and (d) 1 V/Å. The dashed white line indicates the boundary of the first Brillouin zone.

before the passage, the electron is in the VB, then after the passage, the electron is completely transferred to the CB, and vice versa. The double passage of the Dirac point leaves the electron in the original state, i.e., in the VB.

Due to this property of the interband coupling, the CB population distribution has the following structure. For a field amplitude as low as 0.002 V/Å, near each Dirac point, there are two hot spots [see Fig. 2(a)], i.e., regions with a large CB population, one above and another below the Dirac point. They are separated by dark regions, which, as mentioned above, are due to singularity of the dipole matrix elements at the Dirac points. With increasing field amplitude each bright spot transforms into a set of dark and bright fringes [see Figs. 2(b)–2(d)], which are due to interference effects. The first appearance of such an interference pattern occurs at a field amplitude of $F_0^{(1)}$, which can be calculated as

$$F_0^{(1)} \approx 2\frac{\hbar\omega^2}{ev_F}, \tag{24}$$

where ω is the characteristic carrier frequency of the pulse, and $v_F \sim \alpha c = e^2/\hbar$ is the Fermi velocity of electrons. For $\hbar\omega \approx 1.6$ eV, we obtain $F_0^{(1)} \approx 0.3$ V/Å. This is in qualitative agreement with the calculation results illustrated in Fig. 2(b)]. Note that the same field amplitude of $\sim F_0^{(1)}$ determines the onset of the saturation of absorbance [cf. Fig. 1(a)]. Additionally, one can also evaluate the separation between the fringes in the reciprocal space, Δk, as

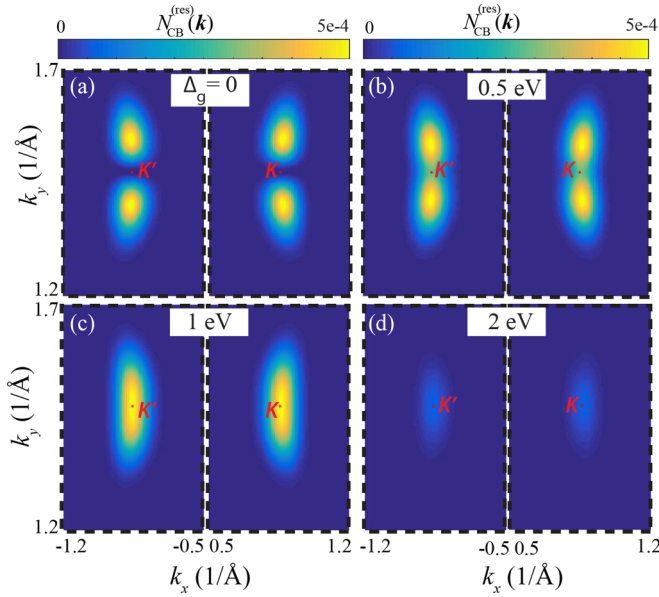$$\Delta k = \frac{2\omega}{v_F}. \tag{25}$$

FIG. 3. Residual CB population distribution for gapped graphene with a bandgap of $\Delta_g = 0$, 0.5, 1, and 2 eV. The optical pulse is linearly polarized along the x direction. The amplitude of the pulse is 0.002 V/Å. The CB population distributions are shown near the K and K' points.

Note that this separation does not depend on the pulse amplitude, which defines the number of fringes estimated as $\approx F_0/F_0^{(1)}$. Estimating from Eq. (25), for $\hbar\omega = 1.6$ eV, we obtain $\Delta k \approx 0.2$ Å^{-1}. This is in good quantitative agreement with Figs. 2(c) and 2(d).

As a function of the bandgap, Δ_g, the absorbance shows different types of behavior at low and high field amplitudes, F_0 (see Fig. 1). At large F_0, $F_0 \gtrsim \Delta_g/a$, where a is the lattice constant, the absorbance is almost independent of the bandgap, while at smaller F_0 the absorbance has a strong nonmonotonic dependence on Δ_g [see Fig. 1(b)]. The origin of such a dependence can be understood from the CB population distribution, which is shown in Fig. 3 for the field amplitude of $F_0 = 0.002$ V/Å and various bandgaps. For small Δ_g, the CB population has two maxima, above and below the K and K' points. As mentioned above, in pristine graphene, i.e., at zero bandgap, these maxima are due to singularities of the interband dipole matrix element at the Dirac points. At a finite bandgap, the interband coupling is regular and has a single maximum at each Dirac point with a maximum value that is inversely proportional to the bandgap. As a result, with increasing bandgap, the CB population distribution transforms from the two-maximum structure near each Dirac point into a single-maximum structure at the Dirac points, which occurs at $\Delta_g \approx 1$ eV. In this case, the absorbance increases with Δ_g [see Fig. 1(b)]. Subsequently, when the bandgap increases further, the interband coupling at the Dirac point decreases, which suppresses both the CB population [see Fig. 3(d)] and the absorbance.

Another parameter of the pulse, which determines the absorbance of the system, is the duration of the pulse, τ, which determines its carrier frequency, $\omega \sim 1/\tau$. The dependence of the absorbance on τ is shown in Fig. 4 for pristine graphene
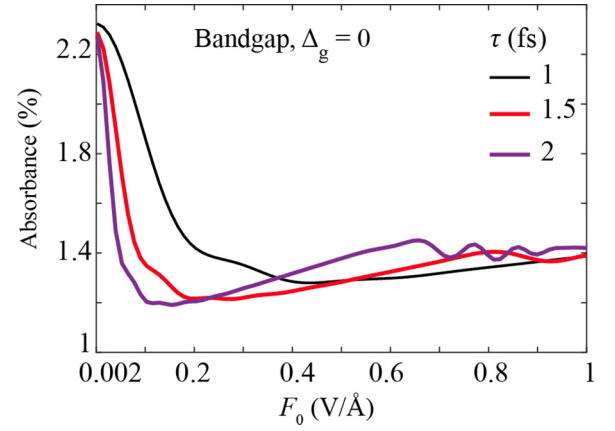

FIG. 4. Absorbance of pristine graphene as a function of the field amplitude for different values of τ: $\tau = 1$, 1.5, and 2 fs.

with a zero bandgap. The results are shown as a function of the field amplitude. We can see in the figure that the saturated value of the absorbance, which is $\approx 1.4\%$ and is achieved at high field amplitudes, does not depend on the duration of the pulse, τ. At the same time, the field amplitude at which the saturated value is achieved depends on τ. Namely, with increasing τ (or a decrease in $\omega \sim 1/\tau$), the saturated value is achieved at a lower field amplitude of F_0. We can reasonably assume that the saturation is also related to the formation of the interference fringes in the electron lattice-momentum distribution. In this case, the field at which the saturation onsets is given by $F_0^{(1)} \propto 1/\tau^2$ [see Eq. (24)]. This scaling is in reasonable agreement with the numerical results in Fig. 4.

B. Circularly polarized ultrafast pulse

Here, we consider the absorption of a single-oscillation circularly polarized pulse. The profile of the pulse, $\mathbf{F}(t) = \{F_x(t), F_y(t)\}$, is defined by the expressions

$$F_x(t) = F_0(1 - 2u^2)\exp(-u^2),\qquad (26)$$

$$F_y(t) = 2F_0 u \exp(-u^2),\qquad (27)$$

where F_0 is the amplitude of the pulse and $u = t/\tau$.

The absorbance for a circularly polarized pulse is shown in Fig. 5(a) as a function of the field amplitude, F_0, for different bandgaps. The absorbance does not saturate at large values
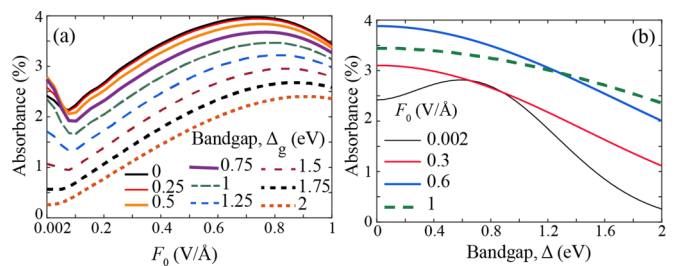

FIG. 5. Absorbance in gapped graphene with a tunable bandgap (a) as a function of the field amplitude for $\Delta_g = 0$, 0.25, 0.5, 0.75, 1, 1.25, 1.5, 1.75, and 2 eV and (b) as a function of the bandgap for $F_0 = 0.002$, 0.3, 0.6, and 1 V/Å. The optical pulse is circularly polarized.
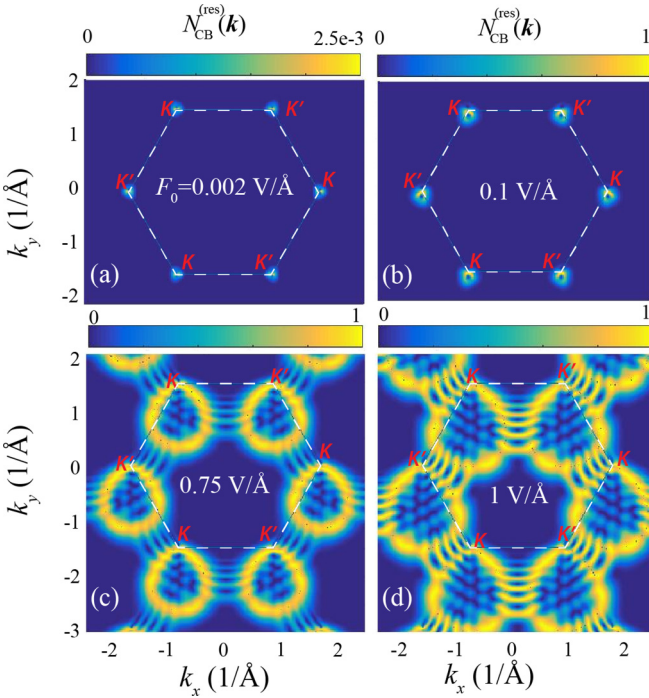
FIG. 6. Residual CB population of graphene with $\Delta_g = 0$ induced by a circularly polarized pulse of different amplitudes: (a) 0.002 V/Å, (b) 0.1 V/Å, (c) 0.75 V/Å, and (d) 1 V/Å. The dashed white line indicates the boundary of the first Brillouin zone.
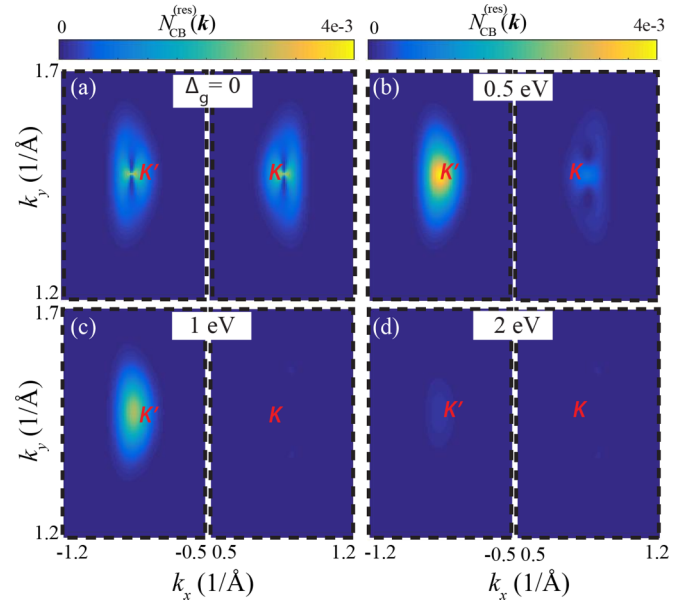

FIG. 7. Residual CB population of gapped graphene induced by a circularly polarized pulse with an amplitude of 0.002 V/Å. The bandgap is (a) 0, (b) 0.5 eV, (c) 1 eV, and (d) 2 eV. The dashed white line indicates the boundary of the first Brillouin zone.

of F_0, in sharp contrast to the case of the linearly polarized pulse. At all field amplitudes, the absorbance has a strong dependence on the bandgap. For small Δ_g, $\Delta_g \lesssim 1.5$ eV, the absorbance first decreases with F_0, reaches its minimum value, and then increases. For large bandgaps, $\Delta_g \gtrsim 1.5$ eV, the absorbance monotonically increases with F_0.

The origin of nonmonotonic dependence of the absorbance at small values of Δ_g can be understood from the CB population distribution shown in Fig. 6 for pristine graphene. At low field amplitudes, $F_0 \lesssim 0.1$ V/Å, the CB population at each Dirac point, K or K', has a single-peak structure localized at the corresponding Dirac point. Within this range of F_0, the absorbance decreases with F_0. Then, at $F_0 \approx 0.1$ V/Å, a single-peak structure of the CB population distribution transforms into an arc that is a caustic, i.e., an image of the separatrix whose size is proportional to F_0 (see Refs. [13] and [33]). With this structure of the CB population, the absorbance increases with F_0. Finally, the absorbance reaches its maximum at $F_0 \approx 0.75$ V/Å. This is the value of F_0 at which the CB population distribution shows the first interference fringes [see Fig. 6(c)]. This interference pattern is clearly visible at high field amplitudes [see Fig. 6(d)]. It is due to the Bloch trajectories crossing the K, K'-valley boundaries, which is likely to limit the absorbance.

Similarly to the case of a linearly polarized pulse, the absorbance for a circularly polarized pulse shows a nonmonotonic dependence on the bandgap at low field amplitudes [see Fig. 5(b)]. Namely, the absorbance first increases with Δ_g and then decreases. This behavior is consistent with the CB population distribution shown in Fig. 7 for the field amplitude $F_0 = 0.002$ V/Å.

IV. CONCLUSIONS

The ultrafast absorption of optical pulses in gapped graphene is determined by specific properties of ultrafast electron dynamics, both intraband and interband, in the field of the pulse. Such dynamics strongly depends on the polarization of the optical pulse, whether it is linear or circular. There is a fundamental difference between these two types of single-oscillation pulses. In fact, the electron Bloch trajectory in the reciprocal space passes twice through the region near the K, K' points (where the interband coupling is large) for linear polarization and only once for circular polarization. As a result, the interference pattern with the dark and bright fringes is clearly visible in the CB population distribution for a linearly polarized pulse, but no such interference is observed at low field amplitudes for a circularly polarized pulse, in agreement with earlier results [13,33]. Due to this effect, the absorption of the linearly and circularly polarized pulses is different. This difference is very pronounced for relatively high field amplitudes, $F_0 \gtrsim 0.1$ V/Å. For low field amplitudes, the absorbance for both types of polarization behaves similarly. This is because, for low field amplitudes, the size of the electron displacement in the reciprocal space is less than or comparable to the size of the region with large interband coupling. In this case, during the whole trajectory, for both linearly and circularly polarized pulses, there is strong (or weak) interband coupling. Thus no interference pattern can be formed, and no difference between linear and circular polarization is observed. Strong polarization dependence of the electron-light interaction has also been demonstrated theoretically in Ref. [49] for continuous light waves, where renormalization of the bandgap of the electron system shows a strong dependence on the light polarization.

At a high field amplitude, when the interference pattern is formed for linearly polarized pulses, the main differences between the circularly and the linearly polarized pulse can be summarized as follows. While for a linearly polarized pulse, the absorbance as a function of the pulse amplitude is saturated at $\approx 1.4\%$, for a circularly polarized pulse, the absorbance does not show any saturation. The absorbance of a circularly polarized pulse can reach a value of as much as 4%. As a function of the bandgap, the absorbance of a linearly polarized pulse has a weak dependence on Δ_g, while the absorbance of a circularly polarized pulse depends strongly on the bandgap.

[1] A. Schiffrin, T. Paasch-Colberg, N. Karpowicz, V. Apalkov, D. Gerster, S. Muhlbrandt, M. Korbman, J. Reichert, M. Schultze, S. Holzner, J. V. Barth, R. Kienberger, R. Ernstorfer, V. S. Yakovlev, M. I. Stockman, and F. Krausz, Optical-field-induced current in dielectrics, Nature **493**, 70 (2012).

[2] V. Apalkov and M. I. Stockman, Theory of dielectric nanofilms in strong ultrafast optical fields, Phys. Rev. B **86**, 165118 (2012).

[3] T. Higuchi, C. Heide, K. Ullmann, H. B. Weber, and P. Hommelhoff, Light-field-driven currents in graphene, Nature **550**, 224 (2017).

[4] E. Gruber, R. A. Wilhelm, R. Pétuya, V. Smejkal, R. Kozubek, A. Hierzenberger, B. C. Bayer, I. Aldazabal, A. K. Kazansky, F. Libisch *et al.*, Ultrafast electronic response of graphene to a strong and localized electric field, Nat. Commun. **7**, 13948 (2016).

[5] S. A. Oliaei Motlagh, V. Apalkov, and M. I. Stockman, Interaction of crystalline topological insulator with an ultrashort laser pulse, Phys. Rev. B **95**, 085438 (2017).

[6] S. A. O. Motlagh, J.-S. Wu, V. Apalkov, and M. I. Stockman, Fundamentally fastest optical processes at the surface of a topological insulator, Phys. Rev. B **98**, 125410 (2018).

[7] C. Heide, T. Higuchi, H. B. Weber, and P. Hommelhoff, Coherent electron trajectory control in graphene, Phys. Rev. Lett. **121**, 207401 (2018).

[8] C. Heide, T. Boolakee, T. Higuchi, H. B. Weber, and P. Hommelhoff, Interaction of carrier envelope phase-stable laser pulses with graphene: The transition from the weak-field to the strong-field regime, New J. Phys. **21**, 045003 (2019).

[9] D. Sun, G. Aivazian, A. M. Jones, J. S. Ross, W. Yao, D. Cobden, and X. Xu, Ultrafast hot-carrier-dominated photocurrent in graphene, Nat. Nanotechnol. **7**, 114 (2012).

[10] H. Mashiko, Y. Chisuga, I. Katayama, K. Oguri, H. Masuda, J. Takeda, and H. Gotoh, Multi-petahertz electron interference in Cr:Al$_2$O$_3$ solid-state material, Nat. Commun. **9**, 1468 (2018).

[11] H. J. Shin, V. L. Nguyen, S. C. Lim, and J.-H. Son, Ultrafast nonlinear travel of hot carriers driven by high-field terahertz pulse, J. Phys. B: At. Mol. Opt. Phys. **51**, 144003 (2018).

[12] M. Trushin, A. Grupp, G. Soavi, A. Budweg, D. De Fazio, U. Sassi, A. Lombardo, A. C. Ferrari, W. Belzig, A. Leitenstorfer, and D. Brida, Ultrafast pseudospin dynamics in graphene, Phys. Rev. B **92**, 165429 (2015).

[13] S. A. Oliaei Motlagh, J.-S. Wu, V. Apalkov, and M. I. Stockman, Femtosecond valley polarization and topological

resonances in transition metal dichalcogenides, Phys. Rev. B **98**, 081406(R) (2018).

[14] D. Sun, J. W. Lai, J. C. Ma, Q. S. Wang, and J. Liu, Review of ultrafast spectroscopy studies of valley carrier dynamics in two-dimensional semiconducting transition metal dichalcogenides, Chin. Phys. B **26**, 037801 (2017).

[15] J. Zhang, H. Ouyang, X. Zheng, J. You, R. Chen, T. Zhou, Y. Sui, Y. Liu, X. Cheng, and T. Jiang, Ultrafast saturable absorption of mos2 nanosheets under different pulse-width excitation conditions, Opt. Lett. **43**, 243 (2018).

[16] Y. S. You, Y. Yin, Y. Wu, A. Chew, X. Ren, F. Zhuang, S. Gholam-Mirzaei, M. Chini, Z. Chang, and S. Ghimire, High-harmonic generation in amorphous solids, Nat. Commun. **8**, 724 (2017).

[17] H. Z. Liu, Y. L. Li, Y. S. You, S. Ghimire, T. F. Heinz, and D. A. Reis, High-harmonic generation from an atomically thin semiconductor, Nat. Phys. **13**, 262 (2017).

[18] A. Kaiser, B. Rethfeld, M. Vicanek, and G. Simon, Microscopic processes in dielectrics under irradiation by subpicosecond laser pulses, Phys. Rev. B **61**, 11437 (2000).

[19] H. G. Rosa, J. A. Castaneda, C. H. B. Cruz, L. A. Padilha, J. C. V. Gomes, E. A. T. de Souza, and H. L. Fragnito, Controlled stacking of graphene monolayer saturable absorbers for ultrashort pulse generation in erbium-doped fiber lasers, Opt. Mater. Express **7**, 2528 (2017).

[20] S. Kumar, M. Anija, N. Kamaraju, K. S. Vasu, K. S. Subrahmanyam, A. K. Sood, and C. N. R. Rao, Femtosecond carrier dynamics and saturable absorption in graphene suspensions, Appl. Phys. Lett. **95** 191911 (2009).

[21] F. Gesuele, Ultrafast hyperspectral transient absorption spectroscopy: Application to single layer graphene, Photonics **6**, 95 (2019).

[22] A. H. Castro Neto, F. Guinea, N. M. R. Peres, K. S. Novoselov, and A. K. Geim, The electronic properties of graphene, Rev. Mod. Phys. **81**, 109 (2009).

[23] D. S. L. Abergel, V. Apalkov, J. Berashevich, K. Ziegler, and T. Chakraborty, Properties of graphene: A theoretical perspective, Adv. Phys. **59**, 261 (2010).

[24] A. K. Geim and K. S. Novoselov, The rise of graphene, Nat. Mater. **6**, 183 (2007).

[25] U. K. Wijewardena, S. E. Brown, and X.-Q. Wang, Epoxy-carbonyl conformation of graphene oxides, J. Phys. Chem. C **120**, 22739 (2016).

[26] S. Withanage, T. Nanayakkara, U. K. Wijewardena, A. Kriisa, and R. G. Mani, The role of surface morphology on nucleation density limitation during the CVD growth of graphene and the factors influencing graphene wrinkle formation, MRS Adv. **4**, 3337 (2019).

[27] U. K. Wijewardena, T. Nanayakkara, R. Samaraweera, S. Withanage, A. Kriisa, and R. G. Mani, Effects of long-time current annealing to the hysteresis in CVD graphene on SiO_2, MRS Adv. **4**, 3319 (2019).

[28] S. Z. Butler, S. M. Hollen, L. Y. Cao, Y. Cui, J. A. Gupta, H. R. Gutierrez, T. F. Heinz, S. S. Hong, J. X. Huang, A. F. Ismach, E. Johnston-Halperin, M. Kuno, V. V. Plashnitsa, R. D. Robinson, R. S. Ruoff, S. Salahuddin, J. Shan, L. Shi, M. G. Spencer, M. Terrones, W. Windl, and J. E. Goldberger, Progress, challenges, and opportunities in two-dimensional materials beyond graphene, ACS Nano **7**, 2898 (2013).

[29] K. S. Novoselov, A. K. Geim, S. V. Morozov, D. Jiang, M. I. Katsnelson, I. V. Grigorieva, S. V. Dubonos, and A. A. Firsov, Two-dimensional gas of massless Dirac fermions in graphene, Nature **438**, 197 (2005).

[30] A. Kormányos, G. Burkard, M. Gmitra, J. Fabian, V. Zólyomi, N. D. Drummond, and V. Fal'ko, k.p theory for two-dimensional transition metal dichalcogenide semiconductors, 2D Mater. **2**, 022001 (2015).

[31] Y. Ye, J. Xiao, H. L. Wang, Z. L. Ye, H. Y. Zhu, M. Zhao, Y. Wang, J. H. Zhao, X. B. Yin, and X. Zhang, Electrical generation and control of the valley carriers in a monolayer transition metal dichalcogenide, Nat. Nanotechnol. **11**, 598 (2016).

[32] D. Jariwala, V. K. Sangwan, L. J. Lauhon, T. J. Marks, and M. C. Hersam, Emerging device applications for semiconducting two-dimensional transition metal dichalcogenides, ACS Nano **8**, 1102 (2014).

[33] S. A. O. Motlagh, F. Nematollahi, V. Apalkov, and M. I. Stockman, Topological resonance and single-optical-cycle valley polarization in gapped graphene, Phys. Rev. B **100**, 115431 (2019).

[34] S. A. O. Motlagh, F. Nematollahi, A. Mitra, A. J. Zafar, V. Apalkov, and M. I. Stockman, Ultrafast optical currents in gapped graphene, J. Phys.: Condens. Matter **32**, 065305 (2019).

[35] M. S. Nevius, M. Conrad, F. Wang, A. Celis, M. N. Nair, A. Taleb-Ibrahimi, A. Tejeda, and E. H. Conrad, Semiconducting graphene from highly ordered substrate interactions, Phys. Rev. Lett. **115**, 136802 (2015).

[36] E. H. Hwang and S. Das Sarma, Single-particle relaxation time versus transport scattering time in a two-dimensional graphene layer, Phys. Rev. B **77**, 195412 (2008).

[37] M. Breusing, S. Kuehn, T. Winzer, E. Malic, F. Milde, N. Severin, J. P. Rabe, C. Ropers, A. Knorr, and T. Elsaesser, Ultrafast nonequilibrium carrier dynamics in a single graphene layer, Phys. Rev. B **83**, 153410 (2011).

[38] E. Malic, T. Winzer, E. Bobkin, and A. Knorr, Microscopic theory of absorption and ultrafast many-particle kinetics in graphene, Phys. Rev. B **84**, 205406 (2011).

[39] D. Brida, A. Tomadin, C. Manzoni, Y. J. Kim, A. Lombardo, S. Milana, R. R. Nair, K. S. Novoselov, A. C. Ferrari, G. Cerullo, and M. Polini, Ultrafast collinear scattering and carrier multiplication in graphene, Nat. Commun. **4**, 1987 (2013).

[40] I. Gierz, J. C. Petersen, M. Mitrano, C. Cacho, I. C. Turcu, E. Springate, A. Stohr, A. Kohler, U. Starke, and A. Cavalleri, Snapshots of non-equilibrium Dirac carrier distributions in graphene, Nat. Mater. **12**, 1119 (2013).

[41] A. Tomadin, D. Brida, G. Cerullo, A. C. Ferrari, and M. Polini, Nonequilibrium dynamics of photoexcited electrons in graphene: Collinear scattering, Auger processes, and the impact of screening, Phys. Rev. B **88**, 035430 (2013).

[42] S. Y. Zhou, G. H. Gweon, A. V. Fedorov, P. N. First, W. A. de Heer, D. H. Lee, F. Guinea, A. H. Castro Neto, and A. Lanzara, Substrate-induced bandgap opening in epitaxial graphene, Nat. Mater. **6**, 770 (2007).

[43] T. G. Pedersen, A.-P. Jauho, and K. Pedersen, Optical response and excitons in gapped graphene, Phys. Rev. B **79**, 113406 (2009).

[44] P. K. Pyatkovskiy, Dynamical polarization, screening, and plasmons in gapped graphene, J. Condens. Matter Phys. **21**, 025506 (2008).

[45] H. Goudarzi, Z. Ahmadi, and A. Jafari, Conduction band population in graphene in ultrashort strong laser field: Case of massive dirac particles, Int. J. Mod. Phys. B **30**, 1650122 (2016).

[46] F. Bloch, Über die Quantenmechanik der Elektronen in Kristall-gittern, Z. Phys. A **52**, 555 (1929).

[47] H. K. Kelardeh, V. Apalkov, and M. I. Stockman, Attosecond strong-field interferometry in graphene: Chirality, singularity, and Berry phase, Phys. Rev. B **93**, 155434 (2016).

[48] W. V. Houston, Acceleration of electrons in a crystal lattice, Phys. Rev. **57**, 184 (1940).

[49] O. V. Kibis, K. Dini, I. V. Iorsh, and I. A. Shelykh, All-optical band engineering of gapped Dirac materials, Phys. Rev. B **95**, 125401 (2017).